

JOINT DEMOSAICKING / RECTIFICATION OF FISHEYE CAMERA IMAGES USING MULTI-COLOR GRAPH LAPLACIAN REGULARIZATION

Fengbo Lan^{*}, Cheng Yang^{*}, Gene Cheung^{*}, Jack Z. G. Tan[†]

^{*}Dept of EECS, York University, Toronto, Canada

[†]Kandao Technology, Sydney, Australia

ABSTRACT

To compose a 360° image from a rig with multiple fisheye cameras, a conventional processing pipeline first performs demosaicking on each fisheye camera’s Bayer-patterned grid, then translates demosaicked pixels from the camera grid to a rectified image grid—thus performing two image interpolation steps in sequence. Hence interpolation errors can accumulate, and acquisition noise in the captured pixels can pollute neighbors in two consecutive processing stages. In this paper, we propose a joint processing framework that performs demosaicking and grid-to-grid mapping simultaneously—thus limiting noise pollution to one interpolation. Specifically, we first obtain a reverse mapping function from a regular on-grid location in the rectified image to an irregular off-grid location in the camera’s Bayer-patterned image. For each pair of adjacent pixels in the rectified grid, we estimate its gradient using the pair’s neighboring pixel gradients in three colors in the Bayer-patterned grid. We construct a similarity graph based on the estimated gradients, and interpolate pixels in the rectified grid directly via graph Laplacian regularization (GLR). Experiments show that our joint method outperforms several competing local methods that execute demosaicking and rectification in sequence, by up to 0.52 dB in PSNR and 0.086 in SSIM on the publicly available dataset, and by up to 5.53dB in PSNR and 0.411 in SSIM on the in-house constructed dataset.

Index Terms— Fisheye camera, demosaicking, image rectification, graph signal processing.

1. INTRODUCTION

Known for their ultra-wide fields of view, fisheye cameras play an important role in modern virtual reality (VR) applications [1]. In particular, when constructing a 360° image using a rig with multiple fisheye cameras capturing different viewpoint images [1], a conventional processing pipeline first performs demosaicking [2] on each camera’s captured Bayer-patterned image (*i.e.*, interpolate missing color components at each pixel location), then translates demosaicked pixels from the fisheye image grid to a target rectified image grid for consumption on a head-mounted display. See [1] for a detailed description of the image processing pipeline.

Performing demosaicking and rectification in sequence means that image interpolation is executed *twice*, where at each stage, errors can accumulate, and acquisition noise at the captured pixels can smear neighbors, resulting in correlated noise and degrading output image quality. To alleviate this problem, in this paper we propose a joint processing framework that performs demosaicking and grid-to-grid mapping simultaneously for fisheye camera images. This means that image interpolation is performed only *once*, limiting the effect

of noise pollution during only one interpolation step. *To the best of our knowledge, we are the first to perform joint demosaicking / rectification in the fisheye camera image processing literature.*

Our work shares a similar optimization philosophy with recent efforts on joint demosaicking / denoising (JDD) [3, 4, 5, 6], that seek advantages over traditional separate demosaicking / denoising approaches, by addressing acquisition noise directly during the demosaick process that obscures noise. Our problem is more complicated in that the mapping from the fisheye camera image grid to the rectified image grid typically involves non-integer locations. We address this issue with a graph-based approach that can more flexibly handle irregular sample placements.

Specifically, we first obtain a reverse mapping function from an integer pixel location in the rectified grid to a non-integer, irregular location in the camera’s Bayer-patterned grid. For each adjacent pixel pair in the rectified grid, we estimate its gradient using the pair’s neighboring captured pixel gradients in the Bayer-patterned grid in all three colors, accounting for local inter-color correlations. We construct a similarity graph based on the estimated gradients, and interpolate pixels in the rectified grid directly via *graph Laplacian regularization* (GLR) [7]. Experiments show that our joint method outperforms several competing local methods that execute demosaicking and rectification in sequence, by up to 0.52 dB in PSNR and 0.086 in SSIM on the Multi-FoV dataset [8] and by up to 5.53dB in PSNR and 0.411 in SSIM on the in-house constructed dataset.

Related Work: There are recent efforts to address inverse imaging problems using graph spectral techniques, including image denoising [7], soft decoding of JPEG images [9, 10], bit-depth enhancement [11], image deblurring [12] and join dequantization / contrast enhancement [13]. Though the details of the employed graph-based regularizers differ across applications, the key to good reconstructed image quality remains the same: to appropriately design an underlying graph that captures inter-pixel similarities of the target image patch. Our current work differs from these works in that we estimate the gradient (difference) of a target color pixel pair in the rectified image grid using relevant observed gradients in the Bayer-patterned grid in all three color components.

2. PRELIMINARIES

We define basic definitions in *graph signal processing* (GSP) [14] to facilitate understanding in the sequel. A graph $\mathcal{G} = (\mathcal{V}, \mathcal{E})$ consists of a node set \mathcal{V} of size N and an edge set \mathcal{E} specified by (i, j, w_{ij}) , where $i, j \in \mathcal{V}$ and $w_{ij} \in \mathbb{R}^+$ is a positive weight of an edge (i, j) reflecting the similarity between samples at nodes i and j . We define a symmetric *adjacency matrix* $\mathbf{W} \in \mathbb{R}^{N \times N}$, where $W_{ij} = w_{ij}$ if $(i, j) \in \mathcal{E}$, and $W_{ij} = 0$ otherwise. We next define a diagonal *degree matrix* $\mathbf{D} \in \mathbb{R}^{N \times N}$, where $D_{ii} = \sum_j w_{ij}$. Given \mathbf{W} and \mathbf{D} , we define a *combinatorial graph Laplacian matrix* as $\mathbf{L} = \mathbf{D} - \mathbf{W}$.

This research is partially funded by Kandao Technology.

By assigning sample value $x_i \in \mathbb{R}$ to node i , the ensemble $\mathbf{x} = [x_1 \dots x_N]^\top \in \mathbb{R}^N$ is called a *graph signal* on graph \mathcal{G} . $\mathbf{x}^\top \mathbf{L}_\mathbf{x} \mathbf{x} = \sum_{(i,j) \in \mathcal{E}} w_{ij} (x_i - x_j)^2$ is known commonly as the *graph Laplacian regularizer* (GLR) [7] and is one smoothness measure of signal \mathbf{x} with respect to the underlying graph defined by \mathbf{L} .

3. PROBLEM FORMULATION

3.1. Reverse Mapping of Output-Input Image Grids

From OCamCalib [15], an omnidirectional camera calibration toolbox, we obtain a mapping function, $f: \mathbb{Z}^2 \rightarrow \mathbb{R}^2$, that maps a pixel i 's integer 2D coordinate (i_x, i_y) , $i_x, i_y \in \mathbb{Z}$, in the rectified image grid, to a real 2D coordinate (s_x, s_y) , $s_x, s_y \in \mathbb{R}$, in the fisheye camera Bayer-patterned image grid. See Fig. 1 for an illustration of reverse pixel mapping from two adjacent pixels i and j in the rectified image grid to locations s and t in the Bayer-patterned grid.

In a conventional demosaicking algorithm [16], each color pixel (say red) in an image grid is interpolated as a weighted linear combination of neighboring red pixels. Similarly, we assume that an N -pixel color block in the rectified image grid can be linearly interpolated from an M -pixel neighborhood $\mathbf{y} \in \mathbb{R}^M$ in the Bayer-patterned grid as $\mathbf{H}\mathbf{y}$, where $\mathbf{H} \in \mathbb{R}^{N \times M}$ is a weight matrix used for interpolation. More complex non-linear interpolation methods can also be incorporated into our joint demosaicking / rectification framework—we leave this direction for future work.

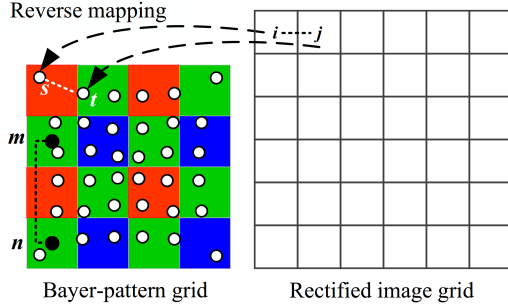


Fig. 1: Reverse mapping from the rectified grid to the Bayer-patterned grid. The white circles at the non-integer location are the mapped locations from the rectified grid. The black circles at the integer location represent for captured pixels in the same color channel on the Bayer-patterned grid. Pixel intensities at these locations are used for estimating the weight between the white circles.

3.2. MAP Formulations for Image Restoration

To reconstruct a target square pixel patch \mathbf{x} in the rectified grid in a chosen color component, we formulate the following optimization given an M -pixel neighborhood \mathbf{y} in the Bayer-patterned grid using GLR [7] as follows:

$$\min_{\mathbf{x}} \|\mathbf{H}\mathbf{y} - \mathbf{x}\|_2^2 + \mu \mathbf{x}^\top \mathbf{L}_\mathbf{x} \mathbf{x} \quad (1)$$

where $\mu > 0$ is weight parameter to trade off the (first) fidelity term with the (second) signal prior. In words, (1) states that the reconstructed signal \mathbf{x} should be similar to interpolation $\mathbf{H}\mathbf{y}$ while being smooth with respect to a graph specified by $\mathbf{L}_\mathbf{x}$.

For fixed interpolation matrix \mathbf{H} and graph Laplacian $\mathbf{L}_\mathbf{x}$, (1) is an unconstrained quadratic programming (QP) problem with solution computed from a system of linear equations:

$$(\mathbf{I} + \mu \mathbf{L}_\mathbf{x}) \mathbf{x} = \mathbf{H}\mathbf{y} \quad (2)$$

Since the coefficient matrix $\mathbf{I} + \mu \mathbf{L}_\mathbf{x}$ in (2) is sparse, symmetric and positive definite (PD), (2) can be efficiently solved without matrix inverse using a fast numerical linear algebra algorithm such as *conjugate gradient* (CG) [17].

3.3. Graph Construction

The restoration performance of (2) depends heavily on how the underlying graph is constructed for target patch \mathbf{x} in the rectified 2D grid, which determines Laplacian $\mathbf{L}_\mathbf{x}$. For connectivity of patch \mathbf{x} , we assume an 8-connected graph, where each pixel in \mathbf{x} is connected to its immediate vertical, horizontal and diagonal neighbors. For edge weight $w_{i,j}$ that connects pixel pair (i, j) in \mathbf{x} , conventionally it is inversely proportional to the *feature distance* of the two corresponding nodes; *i.e.*, the larger the feature distance, the smaller the edge weight [18]. In our imaging scenario, we assume that the feature distance is the magnitude of the estimated *signal gradient* $\Delta_{i,j} \in \mathbb{R}$ between samples i and j . Using an exponential function as the kernel, we can write $w_{i,j}$ as

$$w_{i,j} = \exp \left\{ -\frac{\Delta_{i,j}^2}{\sigma_w^2} \right\} \quad (3)$$

where σ_w is a parameter. (3) implies that $0 \leq w_{i,j} \leq 1$, and the resulting graph Laplacian $\mathbf{L}_\mathbf{x}$, as defined in Section 2, is positive semi-definite (PSD) (see [19] for a proof using Gershgorin Circle Theorem).

The crux of the graph construction procedure thus rests in the gradient estimation for a pixel pair (i, j) . We estimate gradient $\Delta_{i,j} \in \mathbb{R}$ via a *maximum likelihood estimation* (MLE) formulation as follows. Suppose we have access to K noisy observations $\delta_{i,j}^k$ of $\Delta_{i,j}$, $k \in \{1, \dots, K\}$. Then MLE of $\Delta_{i,j}$ given $\delta_{i,j}^k$ is:

$$\max_{\Delta_{i,j}} \Pr \left(\Delta_{i,j} \mid \{\delta_{i,j}^k\}_{k=1}^K \right) \rightarrow \max_{\Delta_{i,j}} \prod_{k=1}^K \Pr \left(\delta_{i,j}^k \mid \Delta_{i,j} \right) \quad (4)$$

where in (4) we assume that each noisy observation $\delta_{i,j}^k$ is generated independently, each with the following distribution:

$$\Pr \left(\delta_{i,j}^k \mid \Delta_{i,j} \right) = \exp \left\{ -v_{i,j}^k (\Delta_{i,j} - \delta_{i,j}^k)^2 \right\} \quad (5)$$

where $v_{i,j}^k$ is a unique parameter for random variable $\delta_{i,j}^k$, to be discussed in details.

Minimizing the negative log of likelihood (4), we get

$$\min_{\Delta_{i,j}} \sum_{k=1}^K v_{i,j}^k (\Delta_{i,j} - \delta_{i,j}^k)^2 \quad (6)$$

To solve (6), we take the derivative with respect to $\Delta_{i,j}$ and set it to 0, resulting in

$$\Delta_{i,j}^* = \frac{1}{V} \sum_{k=1}^K v_{i,j}^k \delta_{i,j}^k \quad (7)$$

where $V = \sum_{k=1}^K v_{i,j}^k$. In other words, the solution (7) is a weighted average of the noisy gradient observations $\delta_{i,j}^k$.

3.4. Noise Model for Inter-pixel Gradient

We obtain K “noisy” gradient observations $\delta_{i,j}$ in our joint demosaicking / rectification framework as follows. We first define a spatial neighborhood $\mathcal{N}_{i,j}$ surrounding non-integer locations s and t in the Bayer-patterned grid that correspond to pixel pair (i, j) in the rectified grid. Within $\mathcal{N}_{i,j}$, we discover $(m, n) \in \mathcal{N}_{i,j}$ that is a pair

of adjacent captured pixels of the same color in the Bayer-patterned grid. We first compute gradient for pair $(m, n) \in \mathcal{N}_{i,j}$:

$$\delta_{i,j}^{m,n} = y_m - y_n \quad (8)$$

where y_m and y_n are the pixel intensity corresponding to the pair (m, n) on the Bayer-pattern \mathbf{y} .

We next compute an associated weight $v_{i,j}^{m,n}$ as:

$$v_{i,j}^{m,n} = \exp \left\{ -\frac{\|\mathbf{l}_s - \mathbf{l}_m\|_2^2 \|\mathbf{l}_t - \mathbf{l}_n\|_2^2}{\sigma_v^2} \right\} \cos \theta_{s,t}^{m,n} \rho_{s,t}^{m,n} \quad (9)$$

where \mathbf{l}_s is the coordinate of pixel s in the Bayer-patterned grid. The pairing of (s, m) and (t, n) is determined by a pre-computed lookup table, using the pixel locations of pairs (m, n) and (s, t) as input. $\theta_{s,t}^{m,n}$ is the angle between line (s, t) and line (m, n) , and σ_v is a parameter. $\rho_{s,t}^{m,n}$ is a *color gradient correlation factor* that estimates the correlation of color gradients between colors of pairs (m, n) and (s, t) , where pairs (m, n) and (s, t) may belong to different color channels. Specifically, when computing ρ for red and blue channels, we reshape the M -pixel Bayer-pattern patch $\mathbf{y} \in \mathbb{R}^{\sqrt{M} \times \sqrt{M}}$ into 4 submatrices $\tilde{\mathbf{y}} \in \mathbb{R}^{\frac{\sqrt{M}}{2} \times \frac{\sqrt{M}}{2}}$ based on color channels, where within each 4-pixel RGGB array on the Bayer-pattern, pixels of green channel in the diagonal location will be considered as 2 independent channels—Green-1 and Green-2. In the case of the red channel, the 2-D correlation coefficient between it and the other 3 channel (Blue, Green-1, Green-2) will be computed as $\rho_{RB}, \rho_{RG_1}, \rho_{RG_2}$, and its self-correlation coefficient $\rho_{RR} = 1$. The coefficient of the blue channel will be computed in the same way. For the green channel, we use the maximum value of the two computed correlation coefficients between it and the other two channels (Red and Blue), *i.e.*, $\rho_{RG} = \max\{\rho_{RG_1}, \rho_{RG_2}\}$ and $\rho_{BG} = \max\{\rho_{BG_1}, \rho_{BG_2}\}$. See Algorithm 1 for a summary of the proposed algorithm.

Algorithm 1 Joint demosaicking / rectification method.

Input: Bayer-pattern image patch \mathbf{y} , \mathbf{H} .

Output: Target image patch \mathbf{x}^* .

- 1: **for** each pair (i, j) on targeted image patch **do**
 - 2: Locating pair (s, t) on Bayer pattern \mathbf{y} with \mathbf{H}
 - 3: Compute the correlation factor ρ with observations in $\mathcal{N}_{i,j}$
 - 4: Compute the gradient $\delta_{i,j}^{m,n}$ and weight $v_{i,j}^{m,n}$ with each pair $(m, n) \in \mathcal{N}_{i,j}$ in three channels with (8) and (9).
 - 5: For each channel, compute the estimated gradient $\Delta_{i,j}^*$ by weighted average via (7).
 - 6: For each $\Delta_{i,j}^*$, compute the edge weight $w_{i,j}$ with (3).
 - 7: **end for**
 - 8: Compute the initial \mathbf{L}_x via $\mathbf{L}_x = \mathbf{D} - \mathbf{A}$.
 - 9: **while** not converge **do**
 - 10: Solving \mathbf{x}^* via (2).
 - 11: Update \mathbf{L}_x^* based on \mathbf{x}^* with (3).
 - 12: **end while**
-

4. EXPERIMENTS

4.1. Experimental Setup

We tested our joint demosaicking / rectification algorithm on a Multi-FoV image dataset [8] and our in-house constructed dataset¹. The Multi-FoV image dataset includes two scenes: `room` and `city`.

¹The dataset is available at: <https://github.com/fengbolan/York-Fisheye-Image-Rectification-Dataset>

Table 1: Average SSIM [21] and PSNR of images from 6 scenes under noise level $\sigma = 15$. 5 and 25 images from `room` and `city` respectively from the Multi-FoV image dataset [8] were used. 3 images each from scene `box`, `chair`, `skull` and `teddy` from our in-house dataset were used. For demosaicking, bilinear interpolation and high quality linear (HQL) method [20] were used for comparison. In both cases, bilinear was used for rectification.

Scene name	SSIM [21]			PSNR (dB)		
	Bilinear	HQL[20]	Proposed	Bilinear	HQL[20]	Proposed
room[8]	0.710	0.702	0.788	20.76	21.04	20.91
city[8]	0.550	0.557	0.622	24.24	24.25	24.77
box	0.599	0.531	0.849	21.88	21.20	22.52
chair	0.601	0.505	0.916	26.68	25.35	29.80
skull	0.648	0.556	0.861	26.02	24.92	27.58
teddy	0.722	0.641	0.919	27.63	26.10	31.63

5 images from `room` and 25 images from `city` were used in our experiment. Our in-house dataset includes 140 pinhole and fisheye camera images generated from 4 publicly available 3-D models: `box`, `chair`, `skull` and `teddy`. 3 images from each scene were used for evaluation. For demosaicking, we employed two competing schemes: 1) bilinear interpolation, and 2) a high quality linear (HQL) filter [20]. For rectification, we employed a bilinear interpolation method. Given a fisheye image, as depicted in Fig. 2a and 3a, we designated a image region that corresponded to the ground truth image (rectified image) as the region of interest (ROI), shown in Fig. 2b and 3b, respectively. We then removed color pixels in the ROI to generate a Bayer-patterned image with additive Gaussian noise (variance $\sigma = 15$) as the input of competing algorithms.

The parameters of our algorithm were set empirically according to the content of the images. μ was set to 1 in all settings. We used 5 iterations for the Multi-FoV dataset images and 8 iterations for the proposed dataset images. σ_w was set to 0.01 in the first iteration and 0.02 in the remaining iterations for the images from the Multi-FoV dataset, and it was set to 0.035 in the first iteration and 0.028 in the remaining iterations for our in-house dataset. σ_u was set to 1.5 for the Multi-FoV dataset and 6 for our in-house dataset. The patch size was set to 32 pixels with a stride of 28 pixels. The experiments were conducted with Matlab R2019a and a computer with a CPU of intel i7-9700T and 32G of RAM.

4.2. Quantitative Comparisons

The visual results for `room` and `city` are shown in Fig. 2 and the results of the in-house dataset are shown in Fig. 3 respectively. The numerical results in average SSIM [21] and PSNR are shown in Table. 1. In Fig. 2e, we observe that due to the proposed smoothness prior employed, compared with the other two methods, the result using our proposed method appears smoother while the boundaries in the image were well preserved. Similar results can be also observed in Fig. 3c-3e, where the noise was noticeable on the image with bilinear and HQL methods, but our proposed method was less affected by such noise. Note that noise in the image demosaicked using the HQL method was more noticeable than the one using the bilinear method. This is because the HQL method employs filters to calculate a gradient map to enhance edges in the image. However, it may also lead to noise enhancement and image quality deterioration. In contrast, our proposed algorithm achieves a good trade-off between edge enhancement and noise reduction.

Such a conclusion is supported by Table. 1. Although PSNR of the HQL method outperformed the bilinear method on the Multi-FoV dataset images, its SSIM was worse than the other two methods.

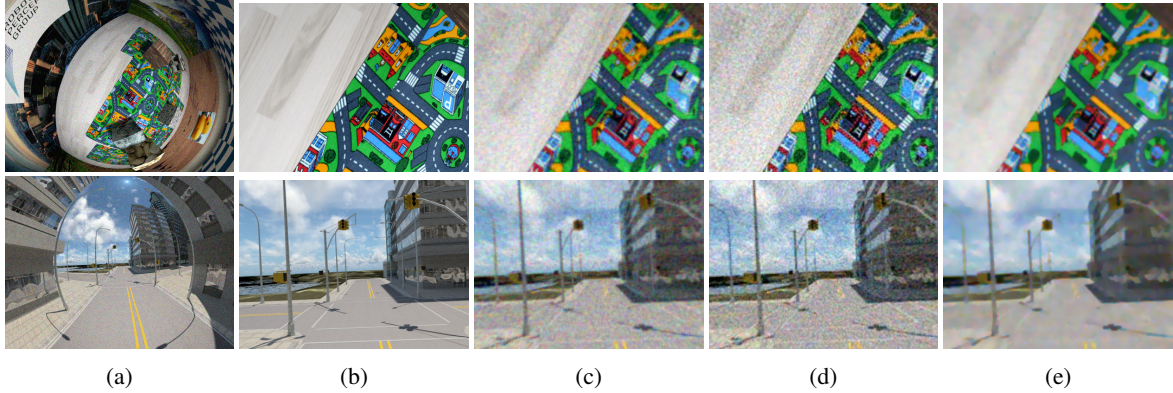


Fig. 2: Results of demosaicking and rectification for *room* and *city* [8]. (a) Ground truth fisheye camera image. (b) Ground truth pinhole image. (c) Demosaicking and rectification using the bilinear method. (d) Demosaicking using high quality linear interpolation (HQL) [20] and rectification using the bilinear method. (e) Our proposed joint demosaicking / rectification method.

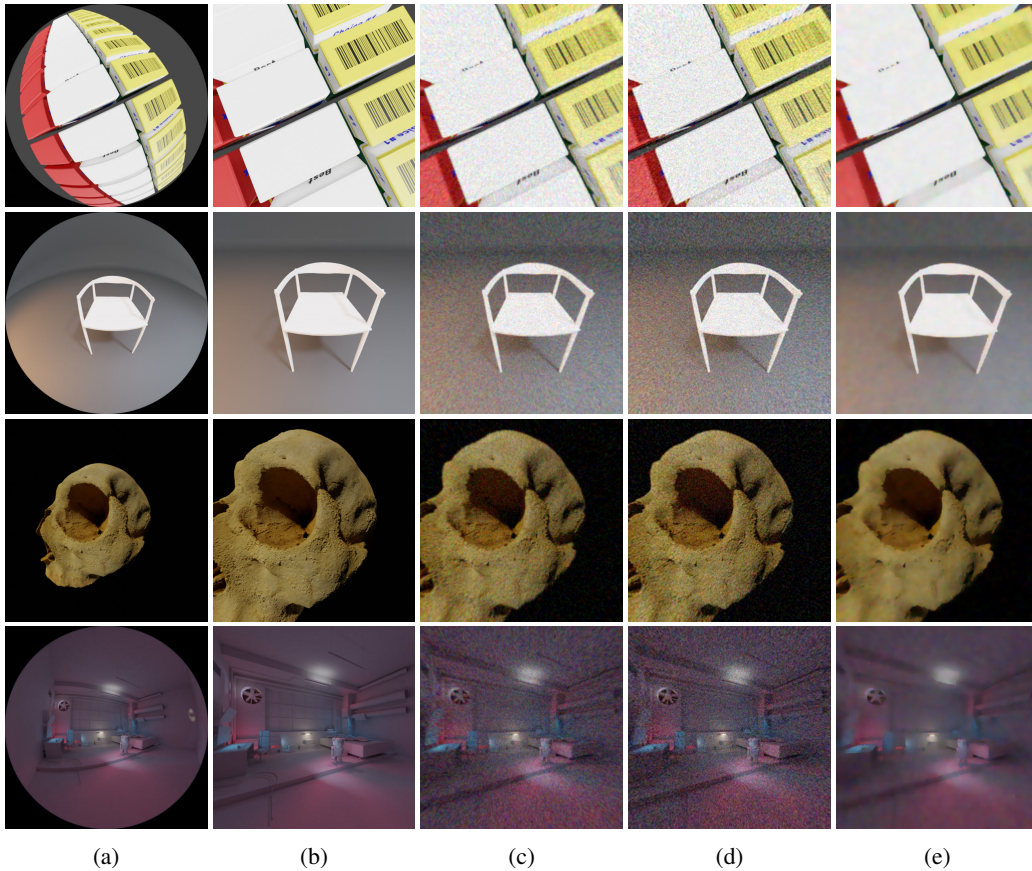


Fig. 3: Demosaicking and rectification result of the in-house dataset, where the images are generated from the 3-D models: *box*, *chair*, *skull* and *teddy*. (a) Ground truth fisheye camera image. (b) Ground truth pinhole image. (c) Demosaicking and rectification using the bilinear method. (d) Demosaicking using HQL interpolation [20] and rectification using the bilinear method. (e) Our proposed joint demosaicking / rectification method.

For the Multi-FoV dataset, PSNR of our proposed method for the *room* images was better than the bilinear method, and it was close to the PSNR of the HQL method. SSIM of our proposed method was higher than the other two methods. For the *city* images, PSNR and SSIM of our proposed method were better than the other two methods. The proposed method outperformed the other two methods

by up to 0.52 dB in PSNR and 0.086 in SSIM, respectively. For our in-house dataset, the proposed method performed well across all images. It outperformed the other two competing methods by up to 5.53dB in PSNR on the images from the scene *teddy*, and up to 0.411 in SSIM on the images from scene *box*.

5. REFERENCES

- [1] J. Tan, G. Cheung, and R. Ma, “360-degree virtual-reality cameras for the masses,” *IEEE MultiMedia*, vol. 25, no. 1, pp. 87–94, Jan. 2018.
- [2] R. Kimmel, “Demosaicing: image reconstruction from color ccd samples,” *IEEE Transactions on Image Processing*, vol. 8, no. 9, pp. 1221–1228, Sep. 1999.
- [3] K. Hirakawa and T. W. Parks, “Joint demosaicing and denoising,” *IEEE Transactions on Image Processing*, vol. 15, no. 8, pp. 2146–2157, Aug 2006.
- [4] L. Zhang, X. Wu, and D. Zhang, “Color reproduction from noisy cfa data of single sensor digital cameras,” *IEEE Transactions on Image Processing*, vol. 16, no. 9, pp. 2184–2197, Sep. 2007.
- [5] M. Gharbi, G. Chaurasia, S. Paris, and F. Durand, “Deep joint demosaicking and denoising,” *ACM Trans. Graph.*, vol. 35, no. 6, pp. 191:1–191:12, Nov. 2016.
- [6] W. Dong, M. Yuan, X. Li, and G. Shi, “Joint demosaicing and denoising with perceptual optimization on a generative adversarial network,” *CoRR*, vol. abs/1802.04723, 2018.
- [7] J. Pang and G. Cheung, “Graph Laplacian regularization for image denoising: Analysis in the continuous domain,” *IEEE Transactions on Image Processing*, vol. 26, no. 4, pp. 1770–1785, April 2017.
- [8] Z. Zhang, H. Rebecq, C. Forster, and D. Scaramuzza, “Benefit of large field-of-view cameras for visual odometry,” in *2016 IEEE International Conference on Robotics and Automation (ICRA)*, May 2016, pp. 801–808.
- [9] X. Liu, G. Cheung, X. Wu, and D. Zhao, “Random walk graph Laplacian-based smoothness prior for soft decoding of JPEG images,” *IEEE Transactions on Image Processing*, vol. 26, no. 2, pp. 509–524, Feb. 2017.
- [10] W. Hu, G. Cheung, and M. Kazui, “Graph-based dequantization of block-compressed piecewise smooth images,” *IEEE Signal Processing Letters*, vol. 23, no. 2, pp. 242–246, 2015.
- [11] P. Wan, G. Cheung, D. Florencio, C. Zhang, and O. C Au, “Image bit-depth enhancement via maximum a posteriori estimation of ac signal,” *IEEE Transactions on Image Processing*, vol. 25, no. 6, pp. 2896–2909, 2016.
- [12] Y. Bai, G. Cheung, X. Liu, and W. Gao, “Graph-based blind image deblurring from a single photograph,” *IEEE Transactions on Image Processing*, vol. 28, no. 3, pp. 1404–1418, March 2019.
- [13] X. Liu, G. Cheung, X. Ji, D. Zhao, and W. Gao, “Graph-based joint dequantization and contrast enhancement of poorly lit JPEG images,” *IEEE Transactions on Image Processing*, vol. 28, no. 3, pp. 1205–1219, March 2019.
- [14] A. Ortega, P. Frossard, J. Kovacevic, J. M. F. Moura, and P. Vandergheynst, “Graph signal processing: Overview, challenges, and applications,” in *Proceedings of the IEEE*, May 2018, vol. 106, no.5, pp. 808–828.
- [15] D. Scaramuzza, A. Martinelli, and R. Siegwart, “A toolbox for easily calibrating omnidirectional cameras,” in *2006 IEEE/RSJ International Conference on Intelligent Robots and Systems*, Oct 2006, pp. 5695–5701.
- [16] A. Davies and P. Fennessy, *Digital imaging for photographers*, Focal Press, 2001.
- [17] M. F. Mller, “A scaled conjugate gradient algorithm for fast supervised learning,” *Neural Networks*, vol. 6, no. 4, pp. 525 – 533, 1993.
- [18] D. I. Shuman et al., “The emerging field of signal processing on graphs: Extending high-dimensional data analysis to networks and other irregular domains,” in *IEEE Signal Processing Magazine*, May 2013, vol. 30, pp. 83–98.
- [19] G. Cheung, E. Magli, Y. Tanaka, and M. K. Ng, “Graph spectral image processing,” *Proceedings of the IEEE*, vol. 106, no. 5, pp. 907–930, May 2018.
- [20] H. S. Malvar, L. He, and R. Cutler, “High-quality linear interpolation for demosaicing of bayer-patterned color images,” in *2004 IEEE International Conference on Acoustics, Speech, and Signal Processing*, May 2004, vol. 3, pp. iii–485.
- [21] Z. Wang, A. Bovik, H. Sheikh, and E. Simoncelli, “Image quality assessment: From error visibility to structural similarity,” in *IEEE Transactions on Image Processing*, August 2005, vol. 13, no.4, pp. 600–612.